文章编号：1001－9014(2019)02－0160－05

DOI:10.11972/j.issn.1001－9014.2019.02.006

A new design of tunable high performance multi-channel optical demultiplexer based on MIM plasmonic ring resonators at telecommunication wavelengths

ZHANG Xue-Wei*, GONG Han-Han

(Northwest Normal University, College of Physics and Electronic Engineering, Lanzhou 730070, China)

Abstract: The tunable high performance multi-channel wavelength demultiplexer (WDM) based on metal-insulator-metal (MIM) plasmonic ring resonators is designed and numerically investigated. By the resonant theory of ring cavity, we find that the channel wavelength of WDM can be easily manipulated by adjusting the radius and refractive index of the ring cavity, which is in good agreement with the results obtained by finite element method (FEM) simulations. The multi-channel WDM structure consisting of a plasmonic waveguide and several ring resonators increases the transmission up to 80% at telecommunication regime, which is two times higher than the results reported in a recent literature. The proposed compact multi-channel wavelength demultiplexer can find more applications for the ultra-compact WDM systems in highly integrated telecommunication circuits.

Key words: surface plasmons, multiplexing, optical resonators, integrated optics devices

PACS: 73.20.Mf, 42.79.Gn, 73.40.Rw

一种新型基于MIM等离子体环形谐振器的可调谐高性能多信道波分解复用器的设计

张雪伟*, 龚韩韩

(西北师范大学 物理与电子工程学院,甘肃 兰州 730070)

摘要:设计并研究了基于金属-介质-金属等离子体环形谐振器的可调谐高性能多通道波分解复用器。通过环形腔的谐振理论分析,发现通过调节环形腔的半径和填充介质折射率可以很容易地控制波分复用器的信道波长,与有限元法模拟得到的结果吻合得很好。由等离子体波导和多个环形谐振器组成的多信道WDM结构增加了在电信波长的传输率,传输率高达80%,比最近文献中报道的结果高出两倍。所设计的多信道波分解复用器在高集成电路中有重要潜在应用。

关 键 词:表面等离子体;解复用器;光学谐振器;集成光器件

中图分类号:O438　　**文献标识码**:A

Introduction

Surface plasmons are the electromagnetic surface waves that travel along the interface between metal and dielectric with an exponential decay to both sides[1]. Surface plasmons polaritons (SPPs) have been widely studied during the past decades because of its ability to overcome the conventional diffraction limit and manipulating light on deep sub-wavelength scales at the same time[2]. Recently, numerous devices based on SPPs such as the all-optical switching, Y-shaped combiners, modulators, sensors, Mach-Zehnder interferometer, directional couplers, splitters, and Bragg reflectors are simulated numerically and demonstrated experimentally[3-9]. The metal-insulator-metal (MIM) structures consist of a dielectric waveguide and two metallic claddings, which strongly confine the incident light in the insulator region[10]. Some devices based on the MIM waveguides have been studied numerically and experimentally, such as the tooth-shaped plasmonic waveguide filters[11], filters based on ring resonators[12] and nanodisk resonator[13],

Received date: 2018-05-10, **revised date**: 2018-12-12　　**收稿日期**:2018-05-10, **修回日期**:2018-12-12

Foundation items:Supported by the Natural Science Foundation of Gansu Province, China(17JR5RA078), the Scientific Research Foundation of Northwest Normal University, China (CX2018Y167)

Biography:ZHANG Xue-Wei (1992-), male, Lanzhou, China, master. Research area involves nano optics and optical circuits.

* **Corresponding author**:E-mail:zhangxuewei2016@163.com

and wavelength selective waveguide[14]. As key factors in the plasmonic filters, optical resonators are crucial structural components of wavelength selective devices due to their symmetry, simplicity, and ease of fabrication.

Based on MIM structures, two types of plasmonic filters, band-pass and band-stop filters have been proposed in previous work. The former allows light with a certain wavelength to pass through the waveguides[12,15] while the latter prohibits a certain wavelength from transmitting[16-18]. Both of these two filters are very important in nanoscale optical devices. However, in some devices such as the (WDM) system, the band-pass filter plays a very important role. WDM plays an important role in signal processing in optical communications. Recently, Huang et al. had proposed a WDM on the basis of nanocapillary resonators[19]. Wang *et al.*[20] had proposed a WDM on the nanodisk resonators. Naghizade S *et al.*[21] and Zhao *et al.*[22] had proposed a compact and high-resolution plasmonic wavelength demultiplexer.

In this paper, a new kind of tunable high performance multi-channel WDM structures based on the ring resonators are proposed and the transmission properties are investigated numerically by using finite element method (FEM). The simulation results agree well with the theoretical analysis. This work may have potential applications in highly integrated optical circuits and optical computing.

1 Structure and theories

Multiple ring resonators are widely used in optical filtering. Firstly, here we used a ring resonator to investigate the design consideration of the optical filter. Fig. 1 (a) shows the plasmonic filter structure which is composed of two slits, two semi-infinite metallic clad-dings, and a ring resonator in the middle of the MIM structure. The system is a two-dimension model. The structure is considered invariant along z-direction. The FEM with COMSOL Multiphysics is employed to realize our simulations. The calculated area is divided by Yee's mesh with a size of 2 nm. The FEM with the scattering boundary condition is employed to investigate the transmission characteristics of the structure. The gray and white areas are silver and air, respectively. Two waveguides are coupled by a ring resonator whose outer radius is R_a, and the inner radius is R_b. The radius of the ring is R, which is the average of the inner and the outer radius, $R = (R_a + R_b)/2$, as depicted by the dashed circle in Fig. 1(a). w represents the widths of the waveguides and the ring. d are the coupling lengths between the waveguides and the ring. The insulators in the slit and ring cavity are set as air with refractive index $n = 1$. The metal is assumed as silver, whose complex relative permittivity can be characterized by the well-known Drude model[12]:

$$\varepsilon_m(\omega) = \varepsilon_\infty - \frac{\omega_p^2}{\omega(\omega + i\gamma)} \quad , \quad (1)$$

The parameters for silver can be set as $\varepsilon_\infty = 3.7$, $\omega_p = 9.1$ eV, and $\gamma = 0.018$ eV[12]. The SPPs are excited with inputting a TM polarized plane wave. The transmission is defined as $T = P_{out}/P_{in}$, P_{in} presents the total incident power, and P_{out} is transmission power. The resonating wavelength of the ring resonator can be obtained theoretically by the equation[12,20]:

$$\frac{J_n'(kR_a)}{J_n'(kR_b)} - \frac{N_n'(kR_a)}{N_n'(kR_b)} = 0 \quad , \quad (2)$$

where $k = \omega(\varepsilon_0\varepsilon_r\mu_0)^{1/2}$, μ_0 is the air permeability. $\varepsilon_r = n_{eff}^2/\mu_0$ is the frequency-dependent effective relative permittivity. J_n and N_n are Bessel function of the first kind and second kind with order n respectively. J_n' and N_n' are derivatives of the Bessel functions to the argument (kR). The first and second-order modes are considered in the present paper, which corresponds to the first and second order of Bessel function. From Eq. 2 we can see that the resonance wavelength λ_0 is dominated by R and the refractive index.

According to temporal coupled mode theory, the transmission of the band-pass filter structure can be obtained from Ref. 20.

$$T(\omega) = \frac{(1/\tau_\omega)^2}{(\omega - \omega_0)^2 + (1/\tau_i + 1/\tau_\omega)^2} \quad , \quad (3)$$

where ω is the frequency of incident light, and ω_0 presents the resonance frequency. $1/\tau_i$ and $1/\tau_\omega$ stand for the decay rate of the field induced by the internal loss in the ring cavity and the power escape through the waveguides, respectively. The width of waveguides and the ring w is 50 nm, and the radius of the ring resonator R is 170 nm. The coupling length between the waveguide and the ring resonator d is set as 8 nm. As presented in Fig. 1(b), the transmission spectrum shows that the incident light far from ω_0 is reflected. There exists a transmitted peak at the resonance frequency. From Eq. 3, when $1/\tau_i$ is far less than $1/\tau_\omega$, the on-resonance transmission (i.e., transmission peak) $T_{max} = (1/\tau_\omega)^2/(1/\tau_\omega + 1/\tau_i)^2$ is close to unity. We can find that the transmission spectra around the resonant modes exhibit Lorentzian profiles from Eq. 3. Far from the resonance frequency, the incident mode is completely reflected. The simulation results are in good accordance with the theoretic analysis.

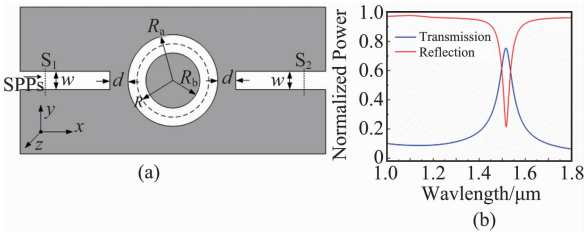

Fig. 1 (a) Schematic diagram of the MIM waveguide with a ring resonator, (b) transmission spectrum of the proposed MIM waveguide with a ring resonator

图 1 (a)MIM 波导环形谐振器原理图,(b)MIM 波导环形谐振器的传输谱

2 Transmission properties of the ring resonator with different parameters

The parameters of the MIM waveguide with a ring resonator structure are set as $d = 8$ nm, $w = 50$ nm, and

$n = 1$. Firstly, we utilize the FEM method to simulate transmission characteristics. Figure 2 (a) shows the transmission spectra pertinent of SPPs corresponding to different radii of the ring resonator. The resonance wavelengths have a red-shift with increasing of the radius. Figure 2(b) reveals that the transmitted-peak wavelength shifts almost have approximately linear relations with the radius of ring cavity. This result is in accordance with the solution of Eq. 2. Since the internal loss in the resonator cannot be neglected, the peaks do not reach 1.0. The internal loss increases when the radius increases. According to the simulations and analysis above, it is seen that the band-pass filter can be easily tuned by changing the radius of ring cavity. The results from the resonant theory of ring cavity are consistent with those obtained by FEM simulations[12-13].

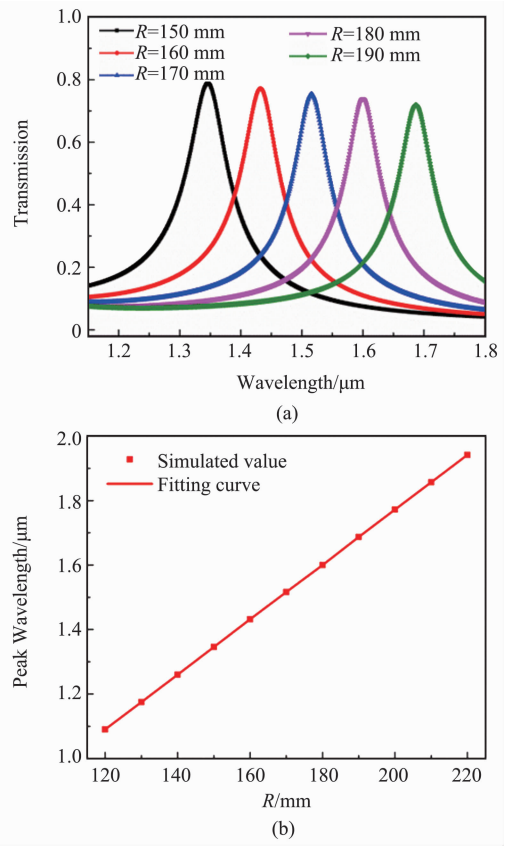

Fig. 2 (a) Transmission spectra for different radius of the ring resonator, (b) transmitted-peak wavelength of the plasmonic filter versus the radius of the ring
图2 (a)不同环腔半径时的透射谱,(b)峰值波长与环腔半径的关系

Successively, we have known that the resonant modes are influenced by the refractive index of the material filling the ring cavity. Thus, we investigate the influence of the material embedded in the resonator on the transmitted-peak wavelength. The radius of the ring cavity is set to be 140 nm. The other parameters are set as above. Figure 3(a) shows the transmission spectra with a different refractive index of the ring cavity. As can be seen from Fig. 3(b), it is found that the transmitted-peak wavelength has a nearly linear relationship with the refractive index n. Therefore, one can simply manipulate the center wavelength of the filter by fitting the material with the appropriate refractive index in the ring resonator.

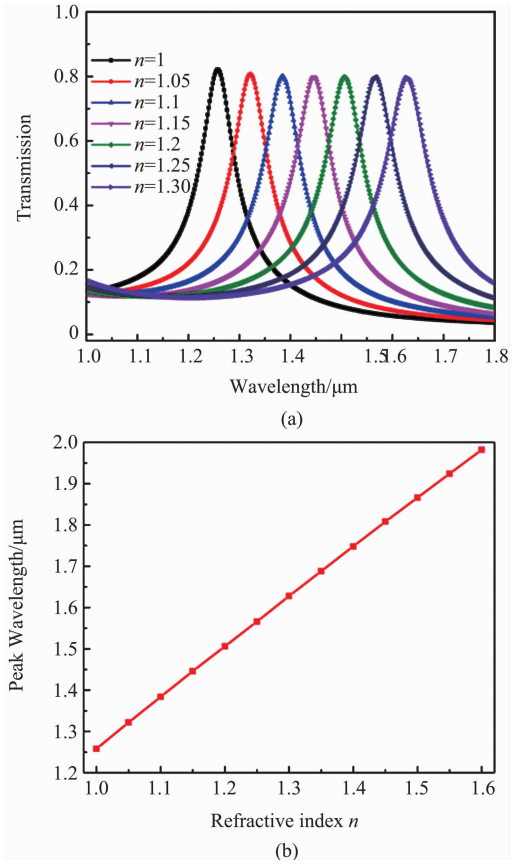

Fig. 3 (a) Transmission spectra of the filter for the different refractive index with $R = 140$ nm, (b) transmitted-peak wavelength of the filter versus refractive index n
图3 (a)不同折射率时的透射谱,(b)透射峰波长与折射率 n 的关系

Another structure parameter d, which stands for the coupling distance between the ring resonator and the waveguides, is an important factor influencing the intensities of transmission spectra. The decay rate $1/\tau_i$ keeps approximately unchanging when only d is changed. Meanwhile, the decay rate $1/\tau_\omega$ will intensively decrease when increased d. The on-resonance transmission T_{max} will accordingly decrease. The results are verified by FEM simulations, as shown in Figs. 4(a-b). According to Eq. 3, full width at half maximum of the resonance spectrum will intensively decrease along with $1/\tau_\omega$, as shown in Fig. 4(a). The resonance wavelengths exhibit slight blue-shift for larger coupling distances, which is consistent with the results in Ref. [13,20]. Therefore, the transmission peaks and bandwidths of the filter can be controlled by changing the coupling length d. This ultra-compact structure has extensive potential in nanoscale integrated optical circuits due to its simplicity for the design of tunable narrow band-pass filters.

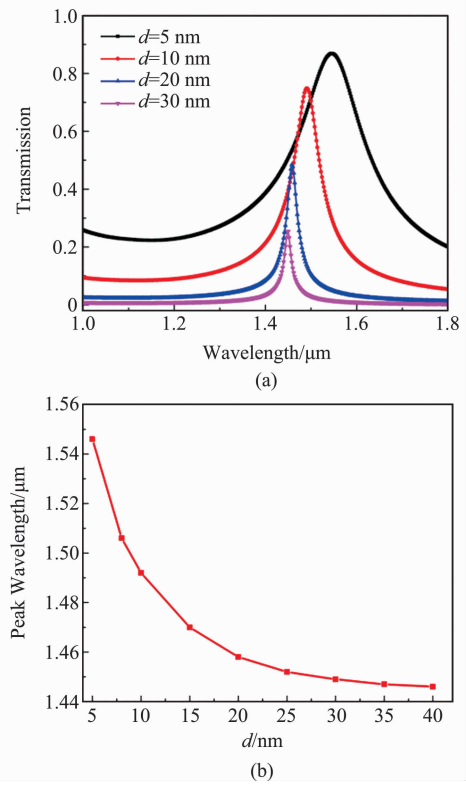

Fig. 4　(a) Transmission spectra for different coupling length d with $R = 140$ nm, $w = 50$ nm, and $n = 1.2$, (b) transmitted-peak wavelength versus the coupling length d

图 4　(a) 耦合距离 d 不同时透射谱,(b) 透射峰波长与 d 的关系

3　Transmission properties of the multi-channel wavelength demultiplexer

According to the above characteristics of the plasmonic filter based on ring resonators, several multi-channel WDM structures are proposed and investigated. Figure 5(a) shows the schematic diagram of the three-channel wavelength demultiplexer. Three rings resonators with different parameters are placed near the waveguide. Here, we mark the ring resonators as cavity I, cavity II, and cavity III. The parameters are set as $R_1 = 160$ nm, $d_1 = 8$ nm, $n_1 = 1.15$, $R_2 = 160$ nm, $d_2 = 8$ nm, $n_2 = 1.05$, $R_3 = 150$ nm, $d_3 = 10$ nm, and $n_3 = 1$. The metallic slit and ring width are 50 nm. The SPPs wave is excited when a TM polarized light is injected into this waveguide from the left port. The power monitors in the three channels are set to record the transmitted power. The transmission of the structure is defined as $T_1 = P_{out1}/P_{in}$, $T_2 = P_{out2}/P_{in}$, $T_3 = P_{out3}/P_{in}$, P_{in} presents the total incident power, P_{out1} is transmission power of port1, P_{out2} is transmission power of port 2 and P_{out3} is transmission power of port3. The transmission spectra of three ports are shown in Fig. 5(b). It is found that the peak of the sharp spectra appears at the resonant wavelength of three ring cavities. This can significantly reduce the required wavelength shift for the plasmonic modulators as well as improve the wavelength resolution for the plasmonic splitters and wavelength demultiplexer. The transmitted-peak wavelengths of three channels for cavity I, cavity II, and cavity III are 1 636, 1 526, and 1 358 nm, respectively.

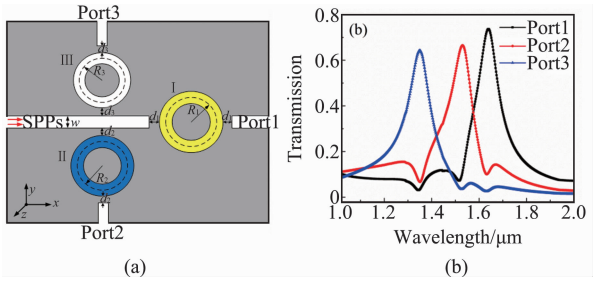

Fig. 5　(a) Schematic diagram of the three-channel WDM, (b) transmission spectra of the three channels WDM

图 5　(a) 三通道 WDM 的原理图,(b) 三通道 WDM 的透射谱

We further design a wavelength demultiplexer with five output channels. Figure 6(a) shows the schematic diagram of the five-channel WDM. We add cavity IV and cavity V into the three-channel wavelength demultiplexer. The parameters of IV and V cavities are chosen as $R_4 = 140$ nm, $d_4 = 10$ nm, $n_4 = 1.0$, $R_5 = 130$ nm, $d_5 = 10$ nm, and $n_5 = 1.0$. Figure 6(b) is the transmission spectra of the five channels WDM. The transmitted-peak wavelength for cavity IV and cavity V are 1 250 nm and 1 162 nm, respectively. Figures 7(a-d) shows the Average field distributions of |Hz| for incident light with the

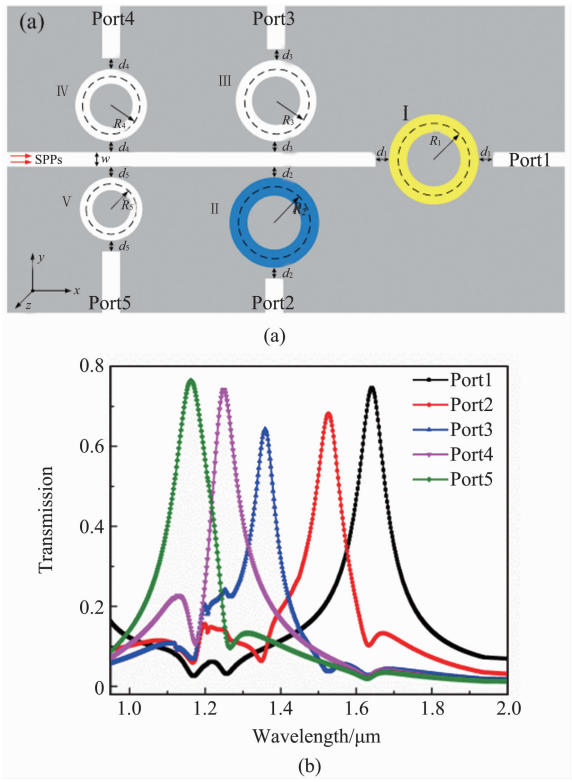

Fig. 6　(a) Schematic diagram of the five-channel WDM, (b) transmission spectra of the five channels WDM

图 6　(a) 五通道 WDM 的原理图,(b) 五通道 WDM 的透射谱

wavelength of 1 636 nm, 1 526 nm, 1 358 nm, and 1 162 nm. It can be seen that the incident lights at 1 636 nm, 1 526 nm, 1 358 nm, and 1 162 nm can pass through cavities I, II, III, and V, which completely covers the wavelength range of the third optical telecommunication window. This is consistent with the transmission spectra shown in Fig. 6(b).

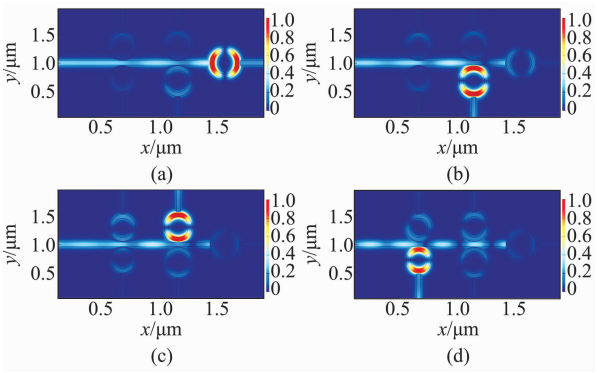

Fig. 7 Average field distributions of $|Hz|$ at different incident wavelengths (a) $\lambda = 1\ 636$ nm, (b) $\lambda = 1\ 526$ nm, (c) $\lambda = 1\ 358$nm, and (d) $\lambda = 1\ 162$ nm, respectively

图 7 对应于入射波长为(a)$\lambda = 1\,636$ nm,(b)$\lambda = 1\,526$ nm,(c)$\lambda = 1\,358$ nm,(d)$\lambda = 1\,162$ nm 时的归一化磁场分布

4 Conclusions

In this paper, a kind of tunable multi-channel wavelength demultiplexer structures based on MIM waveguides with ring resonators is proposed and investigated via FEM. The resonant mode is calculated by the resonant theory of ring cavity, and we find that the central wavelengths of the resonance transmission can be easily controlled by modulating the radius and refractive index of the ring cavity. Furthermore, the wavelengths of the channels can be easily manipulated by changing the geometrical parameters and the refractive index of the ring resonator. It is found that the transmission of some channel can be as high as 80%, rather than about 30% in Ref. 21. The proposed structures may open up new avenues toward the development of demultiplexer and can find important applications in highly integrated optical circuits.

References

[1] Barnes W L, Dereux A, Ebbesen T W. Surface plasmon subwavelength optics [J]. *Nature*, 2003, **424**(6950): 824 - 830.

[2] Zhang Q, Huang X G, Lin X S, *et al*. A subwavelength coupler-type MIM optical filter [J]. *Opt. Express*, 2009, **17**(9): 7549 - 7554.

[3] Chen F, Yao D. Tunable multiple all-optical switch based on multi-nanoresonator-coupled waveguide systems containing Kerr material [J]. *Opt. Commun.*, 2014, **312**(4): 143 - 147.

[4] Wang C, Du C, Yao H, *et al*. Surface plasmon polariton propagation and combination in Y-shaped metallic channels [J]. *Opt. Express*, 2005, **13**(26): 10795 - 10800.

[5] Abadía N, Bernadin T, Chaisakul P, *et al*. Low-Power consumption Franz-Keldysh effect plasmonic modulator [J]. *Opt. Express*, 2014, **22**(9): 11236 - 11243.

[6] Fan H, Charbonneau R, Berini P. Long-range surface plasmon triple-output Mach-Zehnder interferometers [J]. *Opt. Express*, 2014, **22**(4): 4006 - 4020.

[7] Alam M Z, Caspers J N, Aitchison J S, *et al*. Compact low loss and broadband hybrid plasmonic directional coupler [J]. *Opt. Express*, 2013, **21**(13): 16029 - 16034.

[8] Ayad M A, Obayya S S A, Swillam M A. Submicron 1xN ultra wideband MIM plasmonic power splitters [J]. *J. Lightwave Technol.*, 2014, **32**(9): 1814 - 1820.

[9] Ortegamoñux A, Richter I, Schmid J H, *et al*. Design of narrowband Bragg spectral filters in subwavelength grating metamaterial waveguides [J]. *Opt. Express*, 2018, **26**(1): 179 - 194.

[10] Morozov Y M, Lapchuk A S, Fu M L, *et al*. Numerical analysis of end-fire coupling of surface plasmon polaritons in a metal-insulator-metal waveguide using a simple photoplastic connector [J]. *Photonics Research*, 2018, **6**(3): 149 - 156.

[11] Chen J, Tao J, Zhang Q, *et al*. Systematical research on characteristics of double-sided teeth-shaped nanoplasmonic waveguide filters [J]. *J. Opt. Soc. Am. B*, 2010, **27**(2): 323 - 327.

[12] Liu D, Wang J, Zhang F, Pan, *et al*. Tunable plasmonic band-pass filter with dual side-coupled circular ring resonators [J]. *Sensors*, 2017, **17**(3): 585.

[13] Lu H, Liu X, Mao D, *et al*. Tunable band-pass plasmonic waveguide filters with nanodisk resonators [J]. *Opt. Express*, 2010, **18**(17): 17922 - 17927.

[14] Kong Y, Lin R, Qian W, *et al*. Active dual-wavelength optical switch-based plasmonic demultiplexer using metal-kerr nonlinear material-metal waveguide [J]. *IEEE Photonics Journal*, 2017, **9**(4): 4501908.

[15] Jeong M Y, Jin Y M, Continuously tunable optical notch filter and band-pass filter systems that cover the visible to near-infrared spectral ranges [J]. *Appl. Opt.*, 2018, **57**(8): 1962 - 1966.

[16] Naglich E J, Guyette A C. Reflection-mode bandstop filters with minimum through-line length [J]. *IEEE Trans. Microwave Theory & Tech.*, 2018, **63**(10): 3479 - 3486.

[17] Zhang H, Shen D, Zhang Y. Circular split-ring core resonators used in nanoscale metal-insulator-metal band-stop filters [J]. *Laser Phy. Lett.*, 2014, **11**(11): 115902.

[18] Amini A, Aghili S, Golmohammadi S, *et al*. Design of microelectromechanically tunable metal-insulator-metal plasmonic band-pass/stop filter based on slit waveguides [J]. *Opt. Commun.*, 2017, **403**: 226-233.

[19] Tao J, Huang X G, Zhu J H. A wavelength demultiplexing structure based on metal-dielectric-metal plasmonic nano-capillary resonators [J]. *Opt. Express*, 2010, **18**(11): 11111 - 11116.

[20] Wang G, Lu H, Liu X, *et al*. Tunable multi-channel wavelength demultiplexer based on MIM plasmonic nanodisk resonators at telecommunication regime [J]. *Opt. Express*, 2011, 19(4): 3513 - 3518.

[21] Naghizade S, Sattariesfahlan S M. Tunable high performance 16-channel demultiplexer on 2D photonic crystal ring resonator operating at telecom wavelengths [J]. *Journal of Optical Communications*, 2018.

[22] Liu H, Gao Y, Zhu B, *et al*. A T-shaped high resolution plasmonic demultiplexer based on perturbations of two nanoresonators [J]. *Opt. Commun.*, 2015, **334**: 164 - 169.